Drinkorn, C., Saynisch-Wagner, J., Uenzelmann-Neben, G., Thomas, M. (2021): Decadal climate sensitivity of contouritic sedimentation in a dynamically coupled ice-ocean-sediment model of the North Atlantic. - Palaeogeography Palaeoclimatology Palaeoecology, 572, 110391.

https://doi.org/10.1016/j.palaeo.2021.110391

Decadal climate sensitivity of contouritic sedimentation in a dynamically coupled ice-ocean-sediment model of the North Atlantic

Catherine Drinkorn[1], Jan Saynisch-Wagner[1], Gabriele Uenzelmann-Neben[2], and Maik Thomas[1,3]

[1]Earth System Modelling, Helmholtz Centre Potsdam, GFZ German Research Centre
[2]Alfred-Wegener-Institut, Helmholtz-Zentrum für Polar- und Meeresforschung, Bremerhaven
[3]Institute of Meteorology, Freie Universität Berlin

April 15, 2021

Abstract

Ocean sediment drifts contain important information about past bottom currents but a direct link between the study of sedimentary archives and ocean dynamics is not always possible. To close this gap for the North Atlantic, we set up a new coupled Ice-Ocean-Sediment Model of the N. Atlantic - Arctic region. In order to evaluate the potential dynamics of the model, we conducted decadal sensitivity experiments. In our model contouritic sedimentation shows a significant sensitivity towards climate variability for most of the contourite drift locations in the model domain. We observe a general decrease of sedimentation rates during warm conditions with decreasing atmospheric and oceanic gradients and an extensive increase of sedimentation rates during cold conditions with respective increased gradients. We can relate these results to changes in the dominant bottom circulation supplying deep water masses to the contourite sites under different climate conditions. A better understanding of northern deep water pathways in the Atlantic Meridional Overturning Circulation (AMOC) is crucial for evaluating possible consequences of climate change in the ocean.

1 Introduction

Deep water formation in high latitudes is a key feature of the large scale ocean circulation and essential for the overturning of water masses around the globe.

Newly ventilated waters from polar surfaces are transported into the deep basins of mid-latitudes where they are eventually up-welled again and returned to colder regions as warm surface currents. This circulation is called the Meridional Overturning Circulation (MOC), and in the Atlantic Ocean specifically referred to as the Atlantic Meridional Overturning Circulation (AMOC) (Broeker, 1991). AMOC is not only responsible for the maintenance of regional climate conditions but even more importantly provides a supply of nutrients and oxygen while accounting for a large portion of CO_2-uptake from the atmosphere, especially that of anthropogenic origin (Gruber et al., 2009). In the light of climate change, intense scientific effort is dedicated to possible sensitive responses of this circulation to a warming atmosphere and an increasing freshwater export from the melting polar cryosphere. Reconstructing past ocean states from environmental archives and projecting future scenarios in numerical simulations are two main tools of these investigations (e.g., Stocker et al., 1992; Rahmstorf, 1995).

Sediments are the most important ocean's archives of the distant past: Sediment cores are the basic source for paleo-climate reconstructions based on oxygen isotopes (e.g., Lisiecki and Raymo, 2005) and together with seismic imaging they provide a glimpse of oceanic conditions present millions of years ago by means of a constantly evolving pool of methods (Rothwell and Rack, 2006). Sedimentologists have to take various sediment sources into account in order to derive concepts of past ocean dynamics and climate conditions. Such information is helpful for a better understanding of the modern ocean circulation and its sensitivity to climate change.

However, reconstructions of ocean dynamics from sediment cores are often non-unique. Consequently, numerous sediment transport models, highly variable in terms of dimensionality, versatility and complexity, have evolved throughout the past decades (Papanicolaou et al., 2008) but the majority of applications cover local problems in shallow water regions (e.g., Blaas et al., 2007; Harris and Wiberg, 1997). Three-dimensional sediment models have rarely been used for sedimentation at the transition between deep ocean and continental shelves where boundary currents form major sediment bodies called contourite drifts (Rebesco et al., 2014). This can be attributed to the necessity of a high vertical bottom resolution (like in coastal sediment applications) over a region covering a large-scale bottom circulation (unlike coastal sediment applications) which is numerically expensive.

In the North Atlantic several contourite drifts (Figure 1) have recorded the activity of deep water masses for millions of years. The Eirik Drift is an elongated contourite drift located at the rise of the southern tip of Greenland (Chough and Hesse, 1984). It is the only contourite drift in the region, which is under the direct influence of deep waters crossing the Denmark Strait, the last being referred to as Denmark Strait Overflow Water (DSOW) (Hunter et al., 2007a). DSOW is mainly fed by the East Greenland Current (EGC) which flows southward along the Eastern shelf of Greenland, providing dense Arctic waters for overflows across the Greenland-Iceland-Scotland Ridge (GISR) (Rudels et al., 2002) as one of a few deep water suppliers to the AMOC (Kuhlbrodt

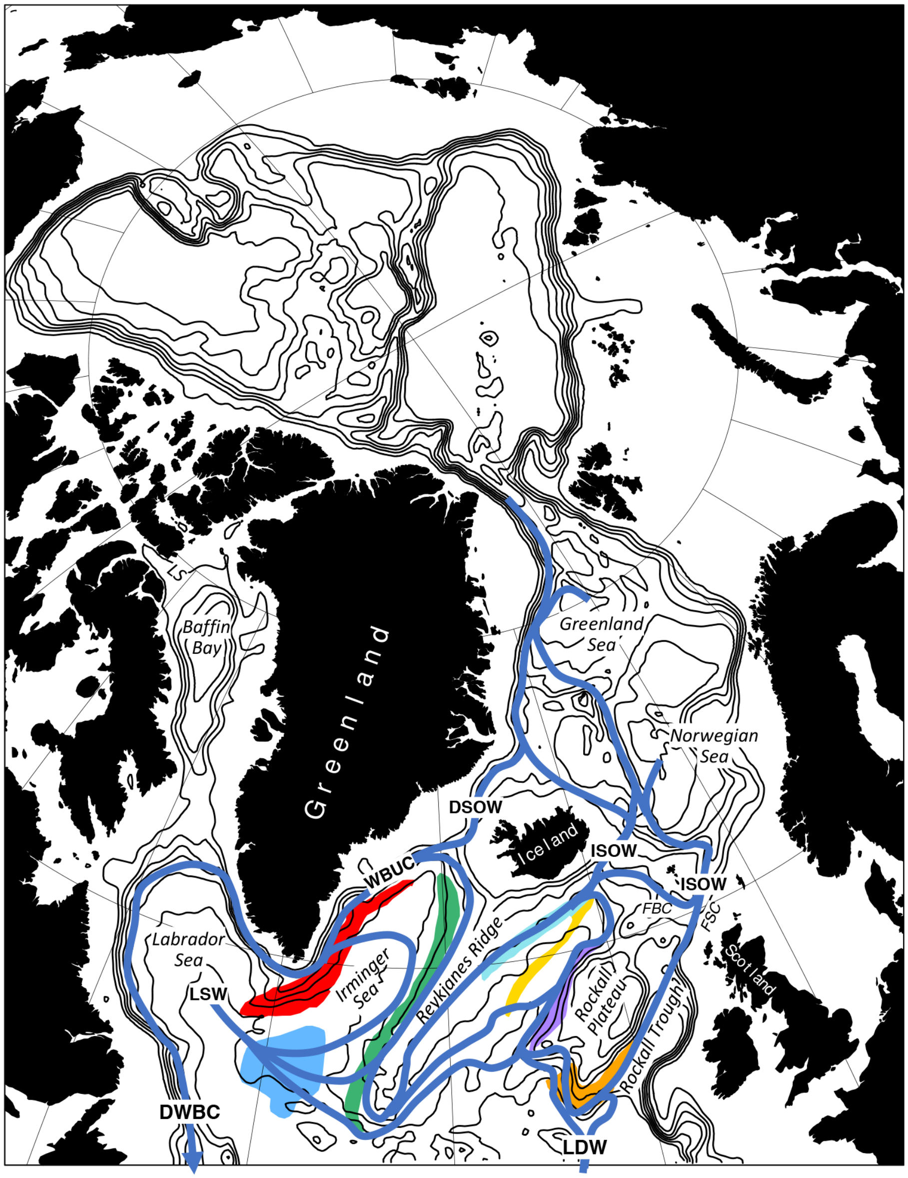

Figure 1: Modeling domain of this study. Thin black lines = 500-3500m isobaths. Position and extend of major contourite drifts south of the Greenland-Iceland-Scotland-Ridge (GISR): Eirik Drift (red, Faugères et al., 1999), Gloria Drift (blue, The US Board on Geographic Names, 2015), Snorri Drift (green, Faugères et al., 1993), Björn Drift (light blue, MacLachlan et al., 2008), Gardar Drift (yellow, MacLachlan et al., 2008), Hatton Drift (purple, MacLachlan et al., 2008), Feni Drift (orange, Stoker, 2002), deep water flows from its suppliers Denmark Strait Overflow Water (DSOW), Iceland-Scotland Overflow Water (ISOW), overflow water through the Faroe Bank Channel (FBC), Labrador Sea water (LSW) and Antarctic Bottom Water (AABW) to the Western Boundary Undercurrent (WBUC). (dark blue lines, after Blake-Mizen et al., 2019; Sivkov et al., 2015; Müller-Michaelis and Uenzelmann-Neben, 2014; Hunter et al., 2007b; Bianchi and McCave, 2000)(LS = Lancaster Sound, FSC = Faroe-Shetland Channel)

et al., 2007). The Eirik Drift is traversed by the Western Boundary Undercurrent (WBUC), a bottom current composed of DSOW, Iceland-Scotland Overflow Waters (ISOW), Labrador Sea Water (LSW) and Lower Deep Water (LDW) (see section 1.1 and Figure 1). Hence, the Eirik Drift is of major importance in the attempt to understand the variability of pathways and intensity of the AMOC.

Numerical experiments along the deep water pathways through the northern North Atlantic can help evaluate the climate sensitivity of the Eirik Drift. Whether an existing coupled ice-ocean-sediment modeling system can be tailored to significantly transfer changes at its lateral and atmospheric boundaries to changes in contourite-scale sedimentary processes via ocean dynamics is the primary subject of this study. Aiming to investigate the role of sea ice and deep water pathways across the GISR and their influence on formation, relocation and retreat of contourite drifts in the northern North Atlantic during different climates, a dynamically coupled ice-ocean-sediment model of the Arctic and Subarctic region was utilized in a new set up. Coupled numerical models have the advantage that, regardless of successful validation with real observations, interdependencies between coupled processes can be concluded from the modeled output. In order to link changes in the structure of deep water flows to sedimentation intensity at a number of different contourite locations, we conducted climate sensitivity studies for a uniform sediment class. With the successful set up of the presented modeling system, conclusions about interactions between ocean dynamics and sedimentation under a dynamically evolving sea ice cover during different climate conditions are derived for the first time.

1.1 Oceanic circulation - Present day and reconstructed

Contourite Drift formation in the region south of the GISR is mainly driven by the WBUC and its suppliers (Hunter et al., 2007a) (Figure 1). Ocean drilling campaigns and seismic surveys, e.g. Ocean Drilling Program (ODP) Leg 105 (Srivastava et al., 1989) and Integrated Ocean Drilling Program (IODP) Leg 303 (Channell et al., 2006), revealed that sedimentation rates and composition have varied throughout the past millions of years by one order of magnitude because of changing locations, intensities and pathways of deep water formation of the AMOC (see review by Hunter et al., 2007b; Stanford et al., 2011; Uenzelmann-Neben and Gruetzner, 2018). The latter study concluded that changes of sea ice cover in the Nordic Seas are potent drivers of the intensity and location of deep convection and may therefore alter contouritic sedimentation driven by deep flows. Haupt et al. (1994) simulated erosion, transport and deposition of a uniform sediment material at the Eirik Drift for the first time. They could verify a significant difference of sedimentation rates and the extent of accumulation between modern conditions and those of the Last Glacial Maximum (26.5 - 19 ky BP) (Clark et al., 2009). However, the various origins of water masses which are pooled in the WBUC traversing the Erik Drift (Müller-Michaelis et al., 2013) make it difficult to decompose causes of those changes:
The EGC mainly feeds DSOW but a substantial part of it is also deflected into the East Icelandic Current (EIC), transporting waters towards overflow

locations east of Iceland where ISOW is formed (Dickson et al., 2008). DSOW and ISOW are often summarized as Nordic Sea Overflow Water (NSOW) (Zou et al., 2020). LDW is a water mass containing modified Antarctic Bottom Water (AABW) (McCartney, 1992). AABW is the densest water mass in the world oceans and accounts for most of the Atlantic Ocean's bottom water. On its way to the North Atlantic AABW mixes with other water masses to become LDW which typically reaches as far north as the southern region of our model domain (Johnson, 2008). LSW, which is almost exclusively formed by deep winter convection in the Labrador Sea, is highly sensitive to long-term climate variability (Bower et al., 2009) and therefore determining its contribution to the different branches of deep circulation is challenging.

A number of reconstructions of overflow waters and their pathways across contourite drifts in the North Atlantic, besides Eirik Drift e.g., Snorri Drift, Björn Drift, Gardar Drift, Hatton Drift, Feni Drift and Gloria Drift (as shown in Figure 1), appear to differ largely in terms of the deep water flows and their interaction (Blake-Mizen et al., 2019; Sivkov et al., 2015; Müller-Michaelis and Uenzelmann-Neben, 2014; Hunter et al., 2007b). The investigation of deep flows across those regions under changing climate conditions has been subject to several numerical and observational studies (e.g., Faugères et al., 1981; Dowling and McCave, 1993; Hunter et al., 2007a; Stanford et al., 2011; Müller-Michaelis and Uenzelmann-Neben, 2014; Langehaug et al., 2016; Blake-Mizen et al., 2019; Zou et al., 2020).

1.2 Structure of the paper

The model setup and its components will be introduced in section 2 along with a detailed description of the experiment procedure. In section 3, we present relative mean deep water flows developed in our simulation and identify prominent deep currents. We also provide sedimentation rates at previously described locations resulting from the conducted experiments. These results will be summarized and put into perspective of the limitation of the model setup which will allow us to compare our results with other observational and numerical studies related to contouritic sedimentation and bottom circulation in the investigated region. In section 4 we will formulate our final conclusions of the study.

2 Methods

A dynamically coupled ice-ocean-sediment model capable of eroding, suspending, transporting and depositing sedimentary materials through the action of ocean circulation was set up or the investigation of sedimentation in the Eirik Drift and six additional drift regions (Figure 1). This model setup reflects the complexity of the investigated processes and their interdependence. As comprehensively described in Rebesco et al. (2013), contouritic sedimentation is fed by deep contour currents driven and shaped under the influence of geostrophic balances, small-scale hydraulics and bottom eddy formation. In the North Atlantic - Arctic region where the role of sea ice on the deep water formation is undisputed, a two-way coupled modeling system comprising ice-ocean-sediment dynamics is therefore necessary. The main parts of the model will be briefly introduced in the following.

2.1 Ice-ocean modeling system

The hydrostatic primitive-equation Regional Ocean Modeling System (ROMS) (Shchepetkin and McWilliams, 2005) was coupled to the sea ice model based on the Norwegian Meteorological Institute's Ice Model (MI-IM) (Røed and Debernard, 2004), embedded into ROMS by Budgell (2005). ROMS operates on an orthogonal curvilinear grid in the horizontal and stretched terrain-following sigma coordinates in the vertical, staggered in an Arakawa C-grid (Arakawa and Lamb, 1977). A domain previously used by Wang et al. (2013) with a horizontal grid size of approximately 20x20 km and 35 vertical layers was reused for this study (Figure 1). The main ice-ocean model setup properties and sources used in this study are summarized in Table 1.

The initial state as well as the open boundary conditions for the South (North Atlantic) and North (Bering Strait) were extracted from the global simulations with the Max Planck Institute Ocean Model (MPIOM) (Jungclaus et al., 2013) conducted for the release 06 (RL06) of the Gravity Recovery and Climate Experiment (GRACE) Atmosphere and Ocean De-Aliasing Level-1B (AOD1B) product (Dobslaw et al., 2017) with respective atmospheric forcing provided by the European Centre for Medium-Range Weather Forecasts (ECMWF) Era-Interim reanalysis archive (Berrisford et al., 2011). Climatological river runoff is based on the R-ArcticNET river discharge dataset for the Pan-Arctic region (Lammers et al., 2001).

2.2 Sedimentation module

In this section, we only provide a short introduction to main features of the sediment module as they were implemented for this study and refer to Warner et al. (2008), who have developed the module for the Coupled-Ocean-Atmosphere-Wave-Sediment Transport (COAWST) Modeling System, for a detailed description.

The sediment module expands ROMS by a domain below the ocean bathymetry consisting of a prescribed sediment class with distinct attributes. Erosion and deposition of sediments are based on conservative material fluxes between the ocean and the sediment bed and act as a source or sink to the advection-diffusion equation for suspended material. Erosion is obtained via a constant erosion rate when a critical erosion stress is exceeded. Deposition occurs as net accumulation sum of erosion and settling flux. Suspended sediments are treated as an additional tracer in the ocean model, thus enabling suspension in the water column and advective-diffusive transport, respectively. The sedimentary processes can evolve the model's bathymetry over time. Suspended sediments are "active" in the sense of altering seawater density in the ocean model. Thus,

Table 1: Overview of the ice-ocean model setup properties and sources used throughout this study. ([1]Wang et al. (2013), [2]Mellor and Yamada (1982), [3]3-hourly ERA-Interim reanalysis data (Berrisford et al. (2011)), [4]analytical based on date, time and location, [5]calculated from 2m-temperature[3] and 2m-dewpoint temperature[3], [6]Lammers et al. (2001), from a global 2001-2010 period simulation for [7]Dobslaw et al. (2017), [8]calculated from 3d momentum[7], [a]Liu et al. (1979) Fairall et al. (1996), [b]Orlanski (1976), [c]Raymond and Kuo (1984), [d]Chapman (1985), [e]Mason et al. (2010), [f]Hunke and Dukowicz (1997), [g]Mellor and Kantha (1989))

Domain	Arctic20km[1]
Horizontal resolution	~ 20 x 20 km
Vertical resolution	~ 0.3 - 240 m
Time step (baroclinic)	20 min
Time step (barotropic)	1 min
Mixing scheme	Mellor-Yamada 2.5[2]
Atmospheric forcing	10m-wind speed[3], 2m-temperature[3], pressure[3] tot. precipitation[3], tot. cloudiness[3], shortwave radiation[4], humidity[5]
Atmos.-ocean fluxes	Bulk flux parameterization[a]
River runoff	Static momentum, temperature and salinity [6]
Open boundaries	Radiative-nudging[b,c] (3d momentum,T,S [7]), Chapman[d] (zeta[7]), Shchepetkin[e] (2d momentum[8])
Ice rheology	Elastic-viscous-plastic[f]
Ice thermodynamics	1-layer with molecular sublayer[g]

the sediment module provides a feedback to the hydrodynamics of the ocean model. There is no further sediment source such as river discharge or pelagic sedimentation in the model other than previously eroded suspended material in the water column.

The overall setup is based on the assumption that any material deposited locally by contouritic sedimentation presumably has been transported by deep currents from further upstream inside the model domain. Therefore, sediment class and model parameters should be regarded as values which enable the formation of contourites in response to simulated deep currents under stable numerical conditions rather than a realistic reconstruction of the particular drifts. With the properties kept constant throughout the experiments, sensitivity behavior towards different climate modes can be derived. An overview of the sediment parameters for the experiments found to enable contouritic sedimentation in the model under stable numerical conditions is given in Table 2.

Table 2: Sediment parameters of the sediment class defined for this study in order to achieve contouritic sedimentation under stable numerical conditions.

Sediment Parameter	Variable	Value
Median grain diameter	D_{50}	$0.2\ \mu m$
Grain density	ρ_s	$2750\ kg\ m^{-3}$
Porosity	ϕ	0.66
Particle settling velocity	w_s	$0.01\ cm\ s^{-1}$
Critical shear of erosion	τ_{ce}	$0.01\ N\ m^{-2}$
Erosion rate parameter	E_0	$0.05 \cdot 10^{-3}\ kg\ m^{-2}s^{-1}$

2.3 Climate sensitivity experiments

Due to the local characteristics of deep water formation in the Subpolar North Atlantic, as profoundly described by Stigebrandt (1985), and topographically advected dense bottom waters (Wåhlin, 2004) driving contouritic sedimentation, the three models were set up with a high resolution across all three dimensions (see Table 1). Hence, baroclinic time steps of the order of minutes were needed to fulfill the Courant-Friedrichs-Lewy (CFL) stability criterion in the split-explicit model. Such a modeling set up consumes large amounts of computer runtime. Therefore, we were seeking to reduce the modeled timespan and were conducting experiments on decadal time scales rather than a centuries long simulation.

Our modeling procedure can be divided into a spinup phase and an experiment phase. During the spinup phase, we were investigating the sedimentation behaviour of a 100-year climatological simulation, starting from initial fields derived from Dobslaw et al. (2017). This simulation was forced with a climatological atmospheric forcing from ERA-Interim reanalysis data (Berrisford et al., 2011) and climatological open boundary inflow based on a global simulation output from Dobslaw et al. (2017). In both datasets, we used data from 2001 to 2010 (see Table 1 for details). In the resulting time series (Figure 2), we identify three phases of the simulated system: 1. A short spinup period of approximately 5 years during which the system quickly reaches a peak sedimentation rate followed by a decrease. 2. An instable phase of variable sedimentation rates on decadal timescales (Figure 2, ∼15-44 model years). 3. A stable phase with a trending sedimentation rate (Figure 2, ∼44-100 model years).

The trending phase exhibits stable sedimentation behavior unlike the other two phases. Therefore, the state of the system within this period was used as a basis for our sensitivity experiments. Aiming to look at relative sensitivity responses in our study, the inherent trend of this phase is neglected. Accordingly, we conducted all following experiments from an initial state starting a few model years before the stable phase begins (i.e., the model year 32), allowing the system to adjust.

In the experiment phase, we conducted three simulations of 38 model years (i.e., until the model year 70) each:

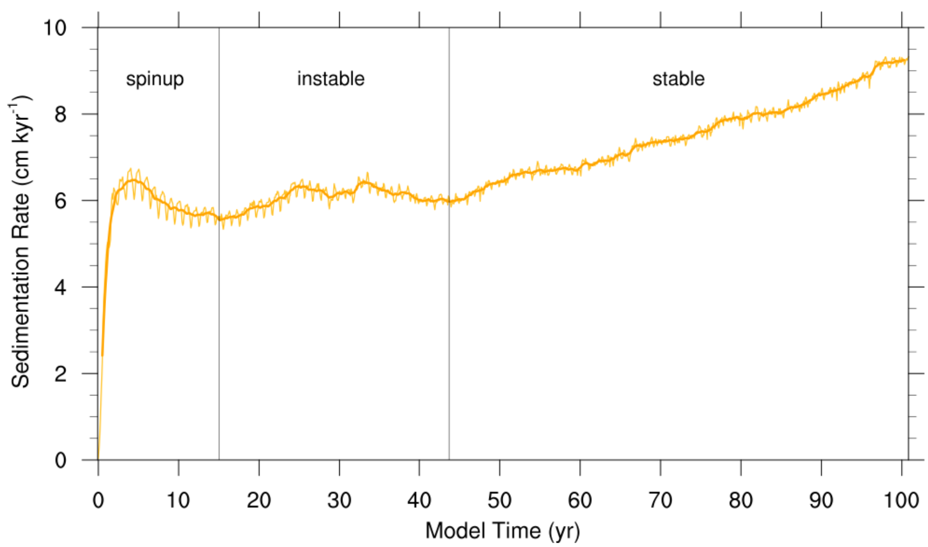

Figure 2: Sedimentation rates averaged over the entire model domain from a 100-year climatological simulation (see CLIM in the following descriptions). The thin orange line represents rates based on monthly model output and the thick line has been produced by applying a 13-month running mean, i.e., removing the seasonal cycle. Thin black vertical lines mark the extent of the three recognized simulation phases: spinup, instable and stable (see main text)

1. CLIM is the climatological run set up for the spin up representing modern climate conditions.
2. JJA is forced by a static mean of the months June, July and August representing lasting warm climate conditions. Compared with annual mean CLIM transports across the respective open lateral boundaries, JJA accounts for
   - +6 % potential advective heat transport from the North Atlantic,
   - +138 % potential advective heat transport from the North Pacific,
   - -10 % potential advective freshwater transport from the North Atlantic,
   - +43 % potential advective freshwater transport from the North Pacific.

   The respective gradients of the potential heat and freshwater supplies between the North Atlantic and the North Pacific from CLIM have been altered by
   - -77 % of the advective heat transport gradient in JJA,
   - -58 % of the advective freshwater transport gradient in JJA.

3. DJF is forced by a static mean of December, January and February representing lasting cold climate conditions. Compared with annual mean CLIM transport across the respective open lateral boundaries, DJF accounts for

   - -2 % potential advective heat transport from the North Atlantic,
   - -81 % potential advective heat transport from the North Pacific,
   - +19 % potential advective freshwater transport from the North Atlantic,
   - -30 % potential advective freshwater transport from the North Pacific.

   The respective gradients of the potential heat and freshwater supplies between the North Atlantic and the North Pacific from CLIM have been altered by

   - +15 % of the advective heat transport gradient in DJF,
   - +65 % of the advective freshwater transport gradient in DJF.

In Figure 3, the mean 2-m temperature, total precipitation and wind vector fields are shown for all three experiments. During JJA, surface temperatures in the atmospheric forcing are larger than or close to zero everywhere except above central Greenland. Consequently, major aerial fronts are mitigated and wind speeds decrease significantly while precipitation ceases. In DJF, the atmosphere is cooled down to well below -20°C above the wider Arctic region and Greenland. In contrast, temperatures above the central Nordic Seas and northern North Atlantic are only decreased by a few degrees Celsius which enhances aerial fronts throughout the model domain leading to a drastic increase in wind speeds. Above the northern North Atlantic and especially in the region of the Icelandic low pressure system to the south of Greenland and Iceland, precipitation is greatly increased while the Arctic Ocean and adjacent continents are exposed to a major arid atmospheric zone due to temperatures well below zero.

In order to quantify the amplification (reduction) of atmospheric fronts in DJF (JJA), we calculated the differences between forcing field mean values for the Arctic region (including the Nordic Seas and Baffin Bay) and the North Atlantic. Masked land areas have not been included since they have no effect on the simulation. The results are summarized in Table 3.

From the modeled output, we obtained mean and relative sedimentation rates and calculated time series of spatially averaged deposition for the contourite drifts shown in Figure 1.

Considering the long time scales of sedimentary processes and the transit times of water masses circulating through the Nordic Seas and Arctic Ocean, it cannot be expected that an equilibrium is reached within the modeled years. However, such a steady state is not necessary in order to reveal anomalies caused by different climate conditions compared to the present state. After removal of

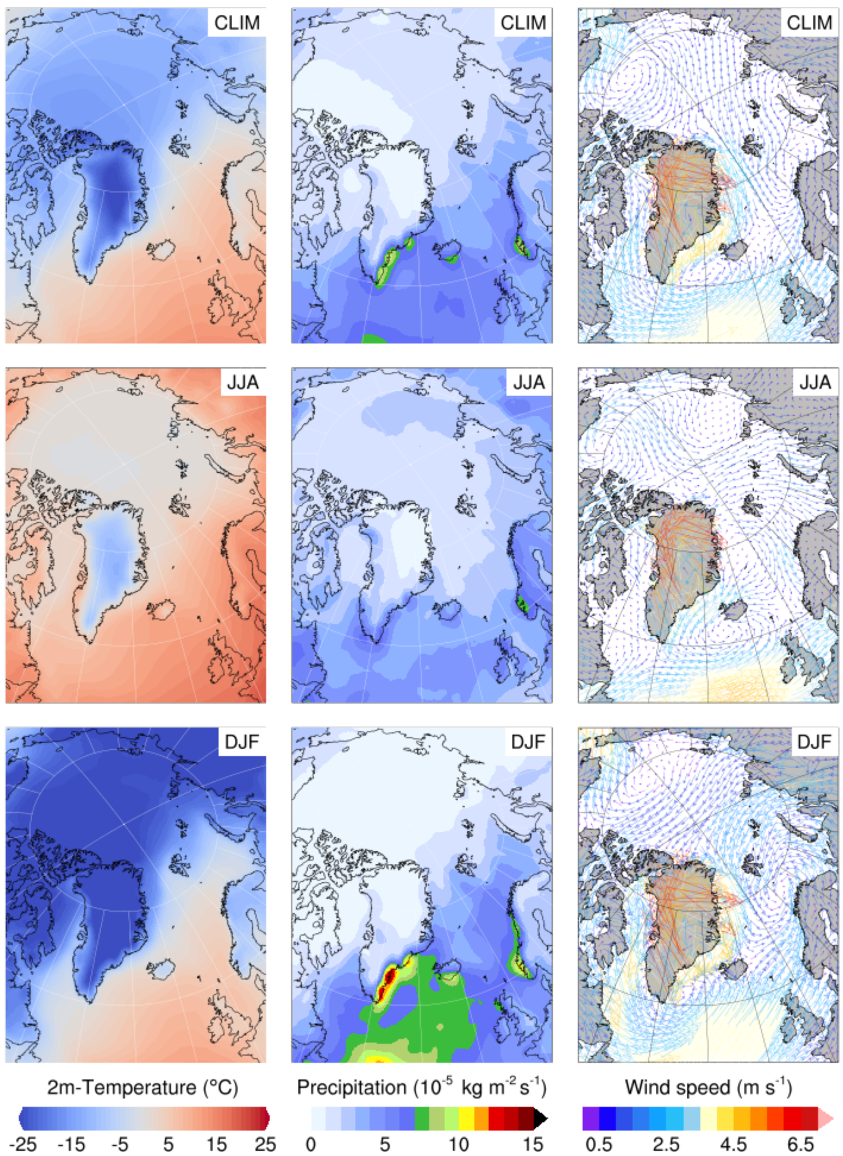

Figure 3: Mean fields of atmospheric forcing in the three experiments CLIM, JJA and DJF: 2-m temperature, total precipitation and wind vector fields based on 3-hourly reanalysis data from 2001 to 2010 of the European Centre for Medium-Range Weather Forecasts (ECMWF) Era-Interim reanalysis archive (Berrisford et al., 2011). CLIM: mean of climatology; JJA: mean of June, July and August in climatology; DJF: mean of December, January and February in climatology.

Table 3: Forcing field mean values (excluding masked land areas) for the Arctic region (including the Nordic Seas and Baffin Bay) and the North Atlantic, and their differences in CLIM (gray shaded cells), ie., the front gradients between the Arctic region and the North Atlantic in the model domain. Gradient cells of increased gradients relative to CLIM are colored red, decreased or reversed gradients relative to CLIM are colored blue.

	Arctic Mean			N. Atl. Mean			|N.Atl. - Arc.|		
	CLIM	DJF	JJA	CLIM	DJF	JJA	CLIM	DJF	JJA
Temp / °C	-3.9	-8.7	1.3	1.3	0.7	2.0	5.2	9.4	0.70
Rain / 10^{-5} kg m^{-2} s-1	0.86	0.80	0.92	0.94	1.20	0.69	0.08	0.40	0.23
|Wind| / m s^{-1}	0.60	0.94	0.42	0.45	0.60	0.35	0.15	0.34	0.07

the trend of the CLIM simulation, remaining shift or drift behavior in JJA or DJF represents the sensitive response to the respective climate condition.

In order to relate changes in sedimentation rates to changes in deep water flows, mean vertically averaged velocity fields were derived from each experiment. Björk et al. (2001) integrated heat and freshwater in the Nordic Seas from the surface to a depth of 500 m in order to capture the upper layer circulation without the shelf regions. The core of the overflows across the Denmark Strait can be found between 400 to 600 m depth (e.g., Köhl et al., 2007; Macrander et al., 2007; Mastropole et al., 2017). Vertically averaging mean deep water velocity fields from a chosen depth of 400 m to the bottom is therefore sufficient as so to capture most of the overflows through the Denmark Strait while excluding upper layer circulation and most of the shelf regions.

3 Results & Discussion

We start this section with an examination of the deep water velocity fields resulting from the sensitivity experiments described in Section 2.3. This is followed by bulk sea ice volumes (Section 3.2). Afterwards, sedimentation in the model domain and time series of spatially averaged sedimentation rates for each contourite drift are presented, allowing us to relate changes in sedimentation rates to previously observed modifications of bottom currents and sea ice volume.

3.1 Deep water currents

Figures 4, 5 and 6 present mean velocity fields vertically averaged over the water column below 400 m. Figure 4 contains the absolute velocity field for the modern climate simulation (CLIM) and figures 5 and 6 the relative velocities of the sensitivity experiments compared to CLIM (i.e., JJA-CLIM and DJF-CLIM).

3.1.1 CLIM

The deep water flows of the CLIM simulation contain a number of well-know deep circulation features in the North Atlantic - Arctic region (compare Figure 1):

- The EGC can be identified as a prominent southward flow along the east Greenland shelf.
- The WBUC commences south of the Denmark Strait and flows along the western rim of the Irminger Sea. Its strongest core is located at the shelf side of Eirik Drift's central flank, mingled with several recirculation features.
- After the WBUC has entered the Labrador Sea and entrained a number of deep waters from various origins, it forms the DWBC, which intensifies on its way to the North Atlantic abyssal. The southern boundary of our model domain ends near Newfoundland with a strong outflow of this deep current.
- Another prominent flow forms east of Reykjanes Ridge, where it commences along the western flank of Björn Drift before it is deflected towards the region north of Eirik Drift. This current can be associated with ISOW.
- The Greenland Sea basin is a known deep convection site in the Nordic Seas Meincke et al. (1997) but a respective convergence gyre is hardly present in the mean deep water vector field of CLIM. A pronounced anticyclonic circulation within the deeper southern basin of the Norwegian Sea, however, can clearly be observed.
- A pronounced current entering the domain south of the Rockall Trough and proceeding westward across the northern North Atlantic could be associated with LDW. Since the above described inflow still exists in the bottom velocity field from just below 3500 m (not shown) we conclude that it must in part contain LDW.

3.1.2 JJA-CLIM

The most notable feature in Figure 5 is the disrupted EGC with a significant weakening of up 50 % compared to CLIM. Consequently, overflows across the Denmark Strait, which are understood to be fed by the EGC under recent climate conditions, are almost inhibited in places. A reduced DSOW under warm climate conditions is in accordance with recent observations (e.g., Macrander et al., 2005).

The convection gyre in the Norwegian Sea is substantially weakened while gyre velocities in the Greenland Sea basin are increased by up to 100 % compared to CLIM. Transports towards the overflow regime east of Iceland are disrupted and tend to recirculate in the region of the Iceland Sea.

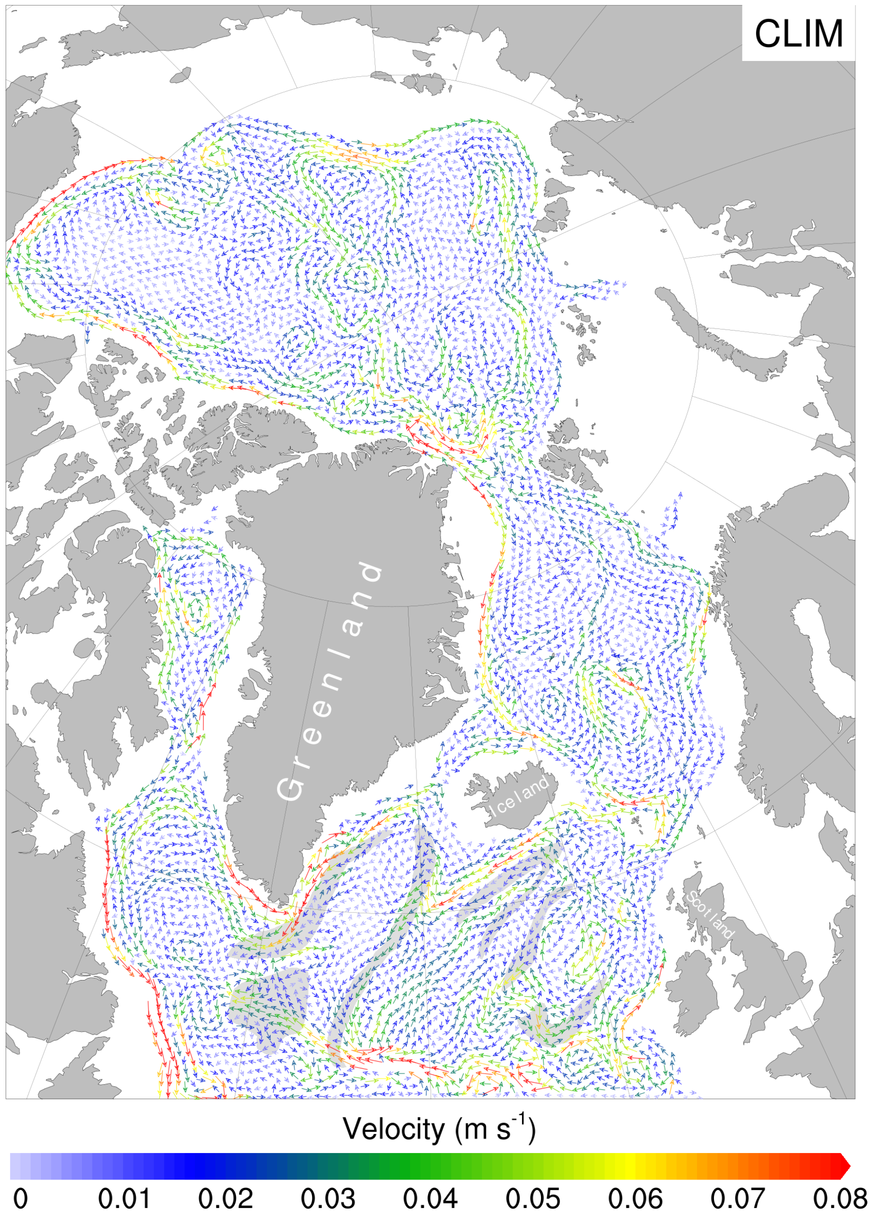

Figure 4: Temporal and vertical mean deep water velocity field from CLIM. The velocity components were averaged vertically from a depth of 400 m to the bottom. The field was limited to a magnitude range from 0.0 to 0.08 m s^{-1}, light gray shaded areas mark the positions of the contourite drifts from Figure 1

Deep water export across most the contourite drifts are generally weaker in JJA, except for Björn Ridge and Gloria Ridge. The transport of LDW towards and over Gloria Drift has increased by up to 100 % of its CLIM magnitudes and the flow aligned to Björn Drift has become slightly stronger compared to CLIM.

3.1.3 DJF-CLIM

In Figure 6 relative deep water flows from DJF are shown. The EGC is strengthened by up to 100 % in places. However, deep water flows through the Denmark Strait are not pronounced. Arctic waters are rather transported to the deeper overflow regime east of Iceland, indicated by a strengthened eastward current north of Iceland with magnitudes of about 100 % more than in CLIM. Consequently, deep water supply via the four westernmost contourite drifts and the northern part of Snorri Drift increases in DJF. This also leads to a generally increased inflow of deep waters to the Eirik Drift and into the erosional channel which exhibits strong recirculation currents under CLIM conditions.

Another striking feature is the weakening of LDW export to Gloria Drift while LSW supply increases drastically. Furthermore, three main sub-currents following different pathways around the southern tip of Greenland, one of which is directed towards the drift, become visible. They are in accordance with three recognized NW-trending secondary ridges of the Eirik Drift which have been associated with the separation of the WBUC at this location (Hunter et al., 2007a,b). In DJF, the southernmost current increases its magnitude by up to 100 % compared to CLIM while the path closer to the shelf is slightly weakened.

3.2 Sea ice volumes

Time series of spatially integrated sea ice volumes over the model domain in CLIM and respective relative sea ice volumes in JJA and DJF are shown in Figure 7. The lower extent of the sea ice volume seasonal cycle in CLIM is in accordance with common results of sea ice models but the upper extent appears to be too low, thus depressing the annual mean values (e.g., Schweiger et al., 2011; Madsen et al., 2016). Changing climate conditions alter the formation of sea ice in the domain: During JJA, sea ice volume quickly decreases within a few model years and finally reaches a relative negative volume corresponding to the mean absolute volume in CLIM, i.e., perennial sea ice in JJA practically vanishes. In DJF it takes the relative sea ice volume in the model domain approximately 15 model years to reach a plateau of almost five times the mean volume in CLIM.

3.3 Sedimentation rates and deep currents at contourite drifts

Detrended mean sedimentation rates in the model domain for CLIM, averaged over the experiment time span defined in section 2, are shown in Figure 8. The

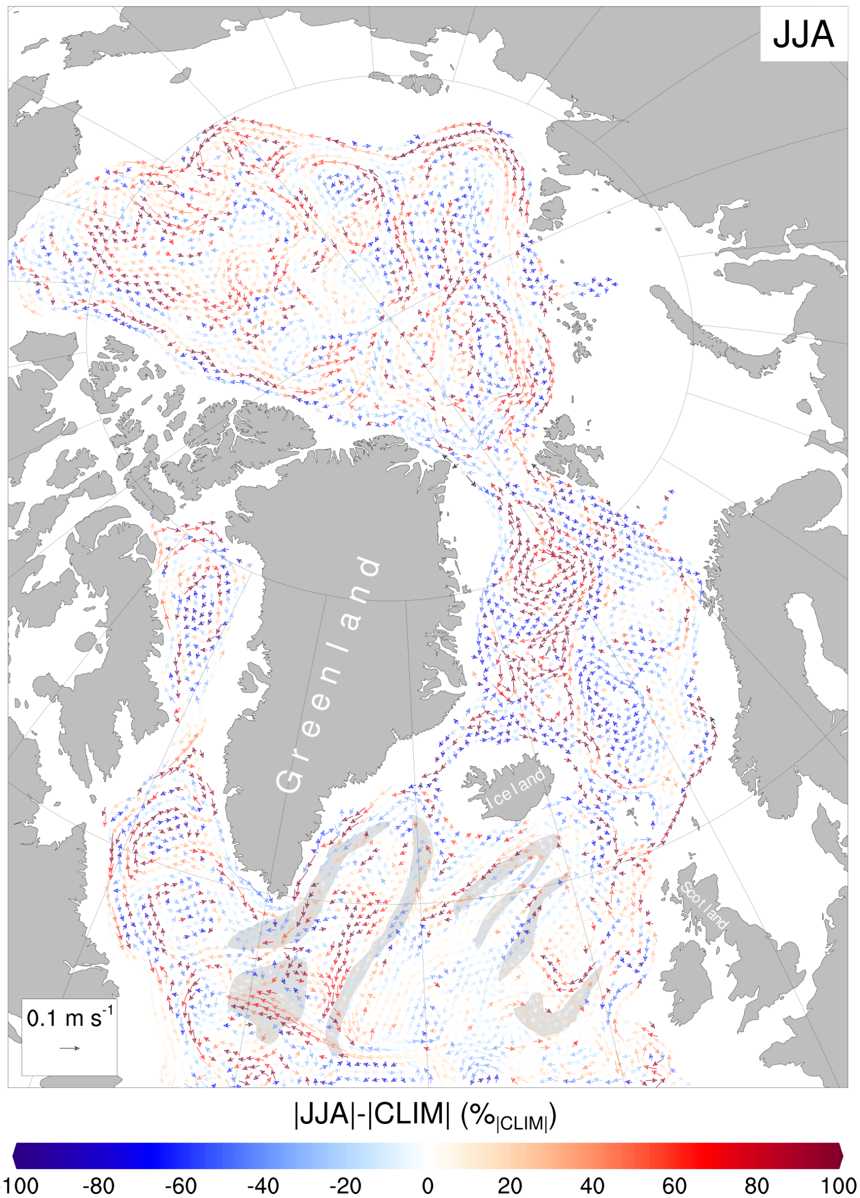

Figure 5: Temporal and vertical mean deep water velocity field from JJA color-coded by the magnitude difference to CLIM as percentage of the latter. The velocity components were averaged vertically from a depth of 400 m to the bottom. Light gray shaded areas mark the positions of the contourite drifts from Figure 1.

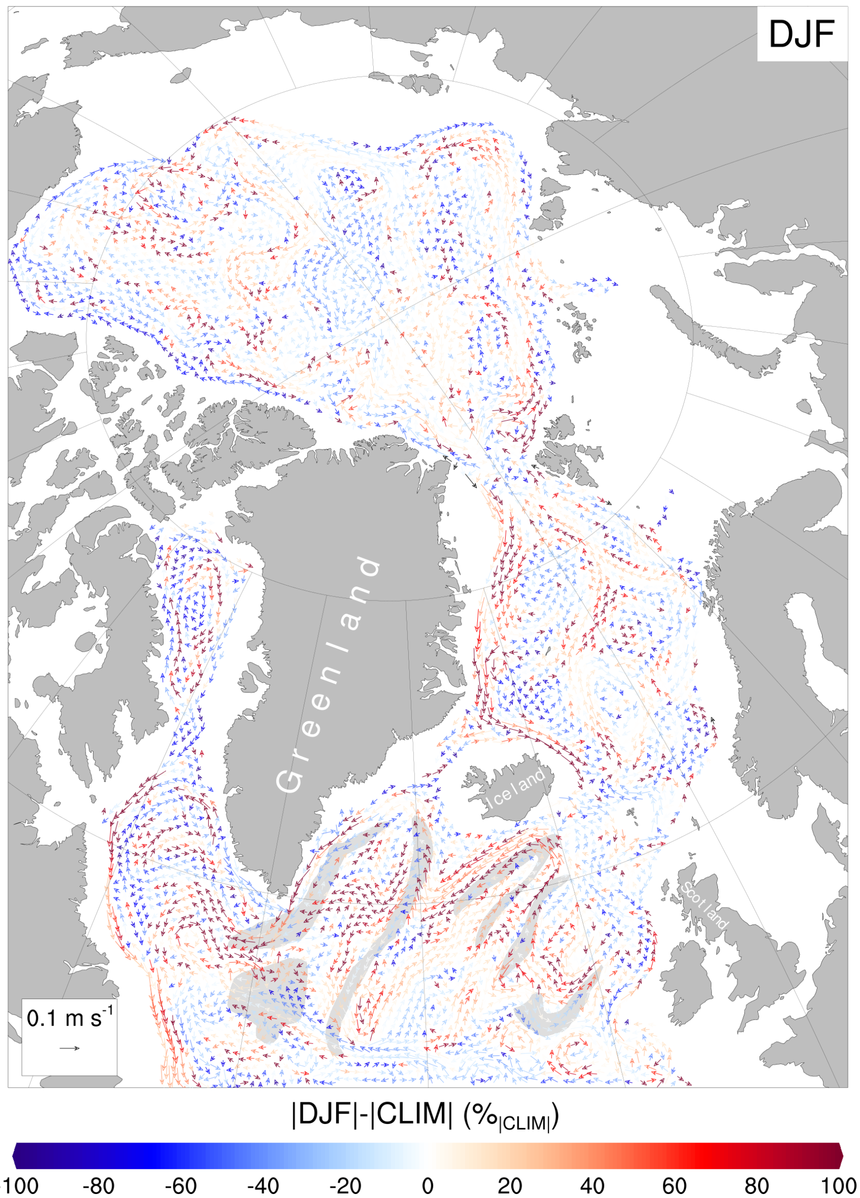

Figure 6: Temporal and vertical mean deep water velocity field from DJF color-coded by the magnitude difference to CLIM as percentage of the latter. The velocity components were averaged vertically from a depth of 400 m to the bottom. Light gray shaded areas mark the positions of the contourite drifts from Figure 1.

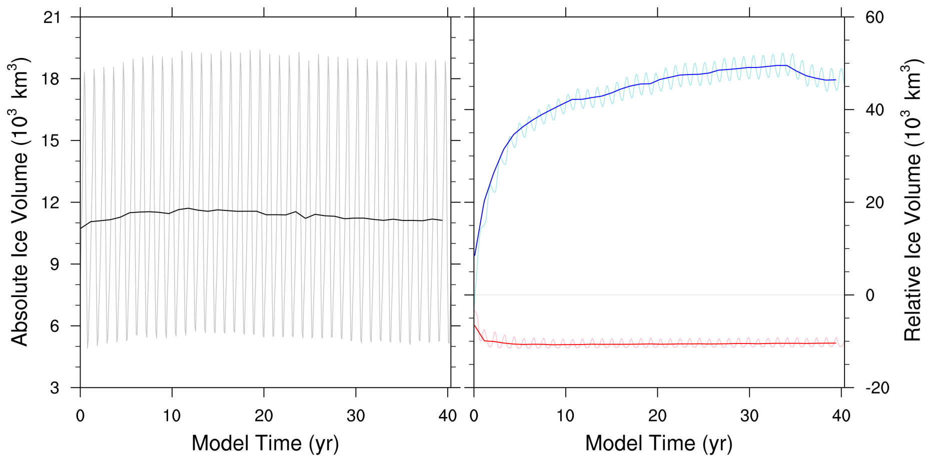

Figure 7: Absolute sea ice volume in CLIM (left panel) and relative sea ice volumes for JJA-CLIM (blue line) and DJF-CLIM (red line) (right panel). Thick lines are annual mean values.

model produces pronounced deposition in the area south of the GISR, especially along contours of the North Atlantic basin. Sedimentation rates at locations of contourite drifts (indicated by white contours in Figure 8) are in the order of respective observations in the region (Parnell-Turner et al., 2015). However, the simulation also exhibits extended accumulation in the deeper troughs of the basins, still following the contours of the bathymetry. Irregular areas and patches of strong erosion correlate with strong bottom currents from Figure 4. Furthermore, the Arctic shelf region show high accumulation rates while patches of strong erosion are located within the narrow strait itself and along the coast of North America.

Figure 9 presents the maximum change of sedimenation rates for JJA and DJF relative to CLIM, i.e., after 38 simulated model years. In order to only asses the change produced by the climate sensitivites, the fields have been detrended with the CLIM trend, respectively. Relative sedimentation in the climate experiments appear to be reversed, with DJF (JJA) showing increased deposition (erosion) in the area south of the GISR and strengthened erosion (deposition) on the Arctic shelf with patches of increased deposition (erosion) in and downstream of the Bering Strait.

In Figures 10 and 11 we present time series of the sedimentation rates at the Eirik Drift and six other drift regions, averaged over the areas indicated in Figures 1 and 8, from the climate sensitivity experiments described in section 2.3. The individual results are discussed in the following subsections.

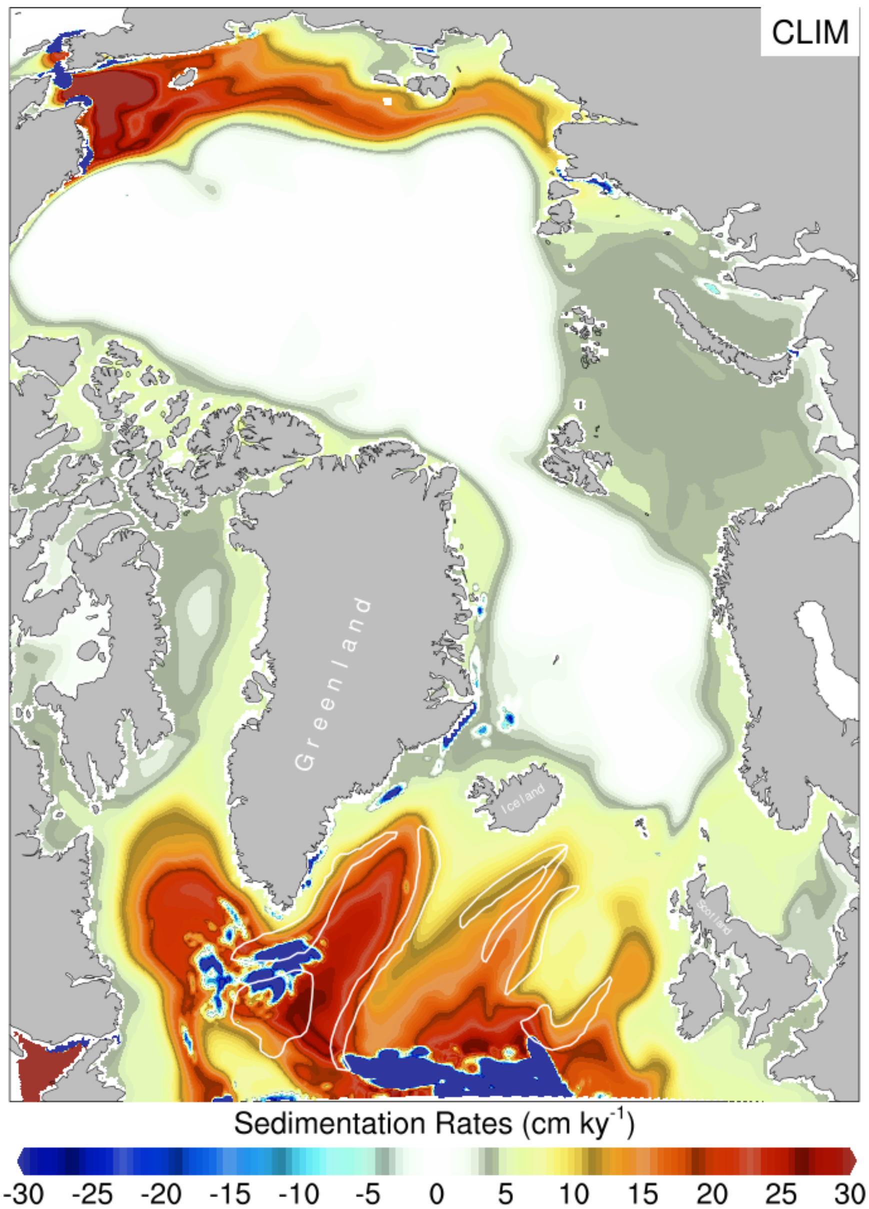

Figure 8: Detrended mean sedimentation rates for CLIM, averaged over the experiment time span defined in section 2 (from model year 32 to 70). Negative values identify locations with mean erosion, locations with positive values exhibit mean deposition. Indicated by the white contours are the positions of the contourite drifts from Figure 1.

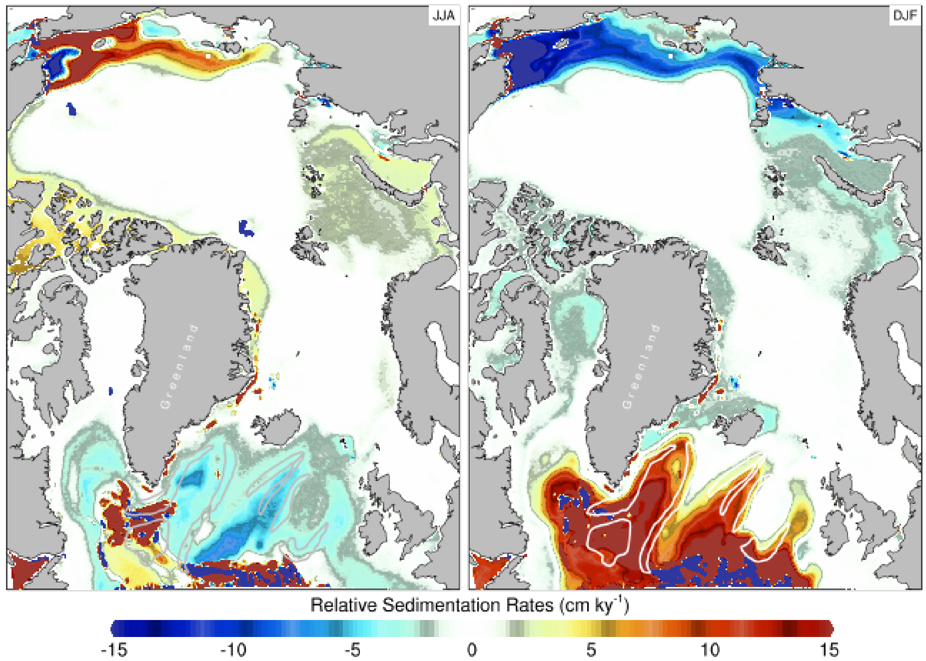

Figure 9: Maximum change in sedimentation rates for JJA (left panel) and DJF (right panel) relative to CLIM. The fields have been detrended with the CLIM trend before. Negative values identify locations with resulting erosion, positive values indicate resulting deposition, relative to CLIM, respectively. Indicated by the grey/white contours are the positions of the contourite drifts from Figure 1.

3.3.1 Eirik Drift

The range of absolute sedimentation rates of the Eirik Drift in Figure 10 (left panel) is in good agreement with known contourite accumulation values of approximately 10-30 cm kyr^{-1} for this region allowing the study of sub-Milankovitch-scale ocean dynamics (Channell et al., 2006). Relative sedimentation rates reveal distinct changes of sedimentation in the Eirik Drift under different climate conditions. JJA induces a significant shift of sedimentation rates towards values of about 2 cm kyr^{-1} lower than CLIM, which is consistent with a reduction of deep currents in places over Eirik Drift observed in the velocity fields for JJA in Figure 5. In contrast, DJF develops a strong drift of increasing sedimentation rates after a cessation phase of about 15 model years while the core of the WBUC strengthens. The initial phase of decreased sedimentation rates in the Eirik Drift corresponds to the timespan of sea ice growth in DJF towards an elevated plateau of a stable volume (Figure 7, right panel). This supports the concept of sea ice extent playing a central role among the causes for increasing sedimentation rates of the Eirik Drift as suggested by Uenzelmann-Neben and

Gruetzner (2018); Müller-Michaelis and Uenzelmann-Neben (2014).

The similarity of the time series' of relative sedimentation rates between Eirik Drift and Snorri Drift (compare Figures 10 and 11) suggest both DSOW and ISOW to be important contributors for sediment supply to the Erik Drift but recent studies suggest that there exist various pathways of ISOW which have not been recognized before (Zou et al., 2020).

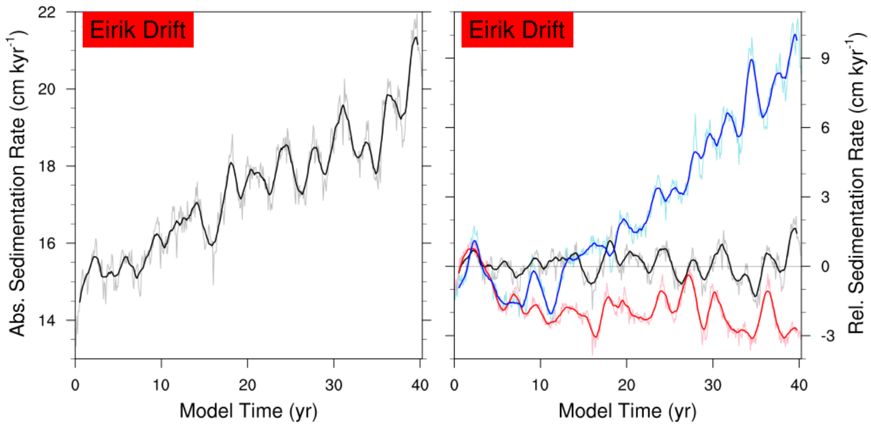

Figure 10: Spatially averaged sedimentation rates in the Eirik Drift for CLIM (left panel), and relative sedimentation rates (i.e., detrended with the CLIM trend) for the experiments JJA (right panel, red lines) and DJF (right panel, blue lines) and the remaining relative variability of CLIM (right panel, black lines), thick lines were smoothed by a 13 months running mean, relative sedimentation rates were obtain by removing the CLIM trend.

3.3.2 Snorri Drift

Snorri Drift is stretched along the western flank of the Reykjanes Ridge and is expected to receive deep waters from the Iceland-Scotland overflows as well as the Labrador Sea at its southern flank. Consequently, under slightly weaker deep currents over central Snorri Drift in JJA, sedimentation shifts towards lower rates in a similar fashion and order as at the Eirik Drift. Intensified deep currents in DJF especially over the northern flank of Snorri Drift are in accordance with a trend towards significantly higher sedimentation rates, respectively.

3.3.3 Björn Drift

On the other side of the Reykjanes Ridge near the overflows east of Iceland resides Björn Drift. Increased deep currents along its northern flank in JJA are not in accordance with the moderate trend towards lower sedimentation rates under these climate conditions. However, moderately higher sedimentation rates

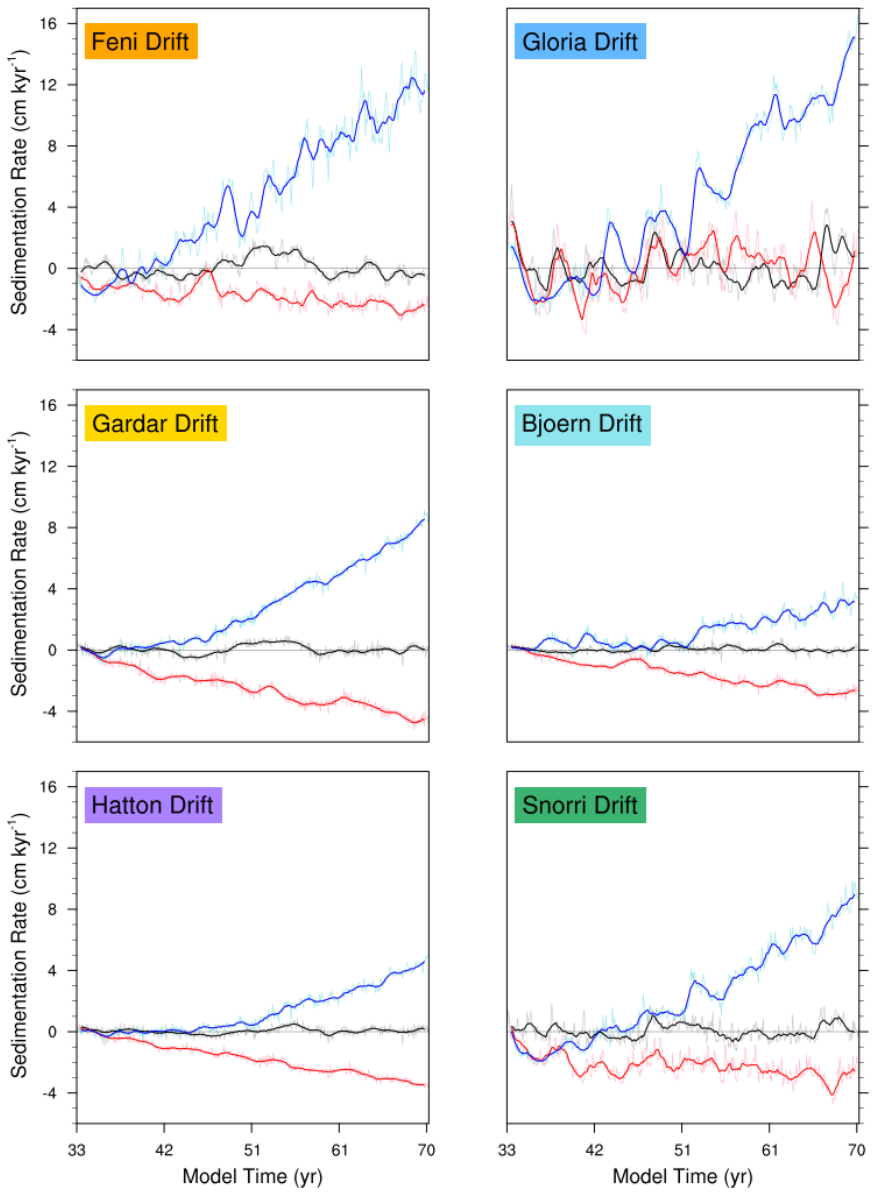

Figure 11: Spatially averaged sedimentation rates per contourite drift region for the experiments CLIM (black lines), JJA (red lines) and DJF (blue lines), thick lines were smoothed by a 13 months running mean and the CLIM trend has been removed from all time series, the colors of the name annotations match the colors of the contourite drifts in Figure 1

in DJF are concurrent with a pronounced strengthening of deep currents above and adjacent to Björn Drift. Hence, the currents along the northern flank may not be part of the bottom circulation but rather belong to water masses at an intermediate depths such has been observed for Labrador Sea Water on top of the overflow water masses from the Nordic Seas (Bianchi and McCave, 2000).

3.3.4 Hatton Drift

Hatton Drift is located at the western margin of the Rockall Plateau and it shows similar relative sedimentation rates as Björn Drift. The moderate increase in DJF cannot directly be associated with a strengthening of deep currents over Hatton Drift. Deep circulation over this location appears to be rather similarly changed in DJF and JJA. However, in the latter experiment Hatton Drift exhibits a trend towards moderately lower sedimentation rates. Like Björn Drift, Hatton Drift is also known to be overflown by LSW at intermediate depths where it can recirculate in the basin of Rockall Trough (Holliday et al., 2000) but there is no respective indication in the deep circulation in DJF or JJA.

3.3.5 Gardar Drift

In the northern Iceland Basin, between Björn and Hatton Drift, lies Gardar Drift which exhibits a strong positive trend in DJF and a moderate negative trend during JJA. In JJA deep currents over Gardar Drift are rather unchanged while velocities for DJF reveal a stronger flow across the drift. These waters most likely originate from the flow around the Rockall Plateau across Feni Drift and Hatton Drift as a secondary source of ISOW. This interpretation is in accordance with Langehaug et al. (2016) who found that bottom velocity at the Gardar Drift shows a high correlation with the volume transport of overflows through the Faroe-Shetland Channel.

3.3.6 Feni Drift

Sedimentation at Feni Drift, located south of the Rockall Plateau, shows a strong trend towards higher rates in DJF while shifting towards slightly lower values under JJA conditions. Deep circulation over the drift appear difficult to decompose in CLIM but partially increasing southward flowing currents at the northern drift flank can be observed in both JJA and DJF. The origin of the strong upward trend under the latter conditions cannot be concluded from the deep water fields only.

3.3.7 Gloria Drift

Since Gloria Drift is mostly traversed by LSW (Hunter et al., 2007a), changes in sedimentation intensity can be linked to modification of the latter. Coherently, strong variations of sedimentation rates throughout the model time are in accordance with the known high inter-annual variability of wintertime deep convection in the Labrador Sea (Avsic et al., 2006). In DJF, the modeling

Table 4: Decadal changes of sedimentation rates at the different drift locations relative to representative changes at the boundaries in terms of field gradients. The cells have been colored according to the magnitudes of change (see the cell color code below).

	Decadal changes of Sedimentation Rates / cm kyr^{-1} per							
	$\Delta T_{\lvert Arc.\text{-}N.Atl.\rvert}$ / °C		Δ Rain$_{\lvert Arc.\text{-}N.Atl.\rvert}$ / kg m^{-2} s^{-1}		ΔHeat$_{N.Atl.\text{-}N.Pac.}$		ΔFresh$_{N.Atl.\text{-}N.Pac.}$	
	DJF (+1.0)	JJA (-1.0)	DJF ($+0.1{\cdot}10^{-5}$)	JJA ($-0.1{\cdot}10^{-5}$)	DJF (+10%)	JJA (-10%)	DJF(+10%)	JJA(-10%)
Eirik Drift	+0.58	-0.24	+0.76	-0.34	+1.61	-0.14	+0.38	-0.18
Gloria Drift	+0.93	+0.08	+1.21	+0.12	+2.57	+0.05	+0.60	+0.07
Snorri Drift	+0.56	-0.23	+0.74	-0.33	+1.56	-0.13	+0.36	-0.18
Björn Drift	+0.13	-0.18	+0.18	-0.25	+0.37	-0.10	+0.09	-0.14
Gardar Drift	+0.51	-0.31	+0.67	-0.46	+1.42	-0.19	+0.33	-0.25
Hatton Drift	+0.28	-0.23	+0.37	-0.33	+0.79	-0.13	+0.18	-0.18
Feni Drift	+0.86	-0.11	1.13	-0.16	+2.40	-0.07	+0.56	-0.09
Cell Colors:	< -0.4	-(0.2-0.4)	> -0.2	< 0.2	0.2-0.4	0.4-0.6	0.6-0.8	0.8-1.0
	1.0-1.5	1.5-2.0	> 2.0					

system induces a significant positive trend of sedimentation in the Gloria Drift while in JJA there is no significant change compared with CLIM. Notably, a prominent convection gyre in the eastern Labrador Sea and an eastward flowing current across Gloria Drift in the DJF deep velocity field are in accordance with the result of strong upward trending sedimentation rates. The role of glacial deep convection in the Labrador Sea and its impact on contouritic sedimentation south of the GISR is suggested by several studies (Fillon and Duplessy, 1980; Dowling and McCave, 1993) and our results are in accordance with their paleo-observations.

3.4 Sedimentation related to changes at the boundaries

Table 4 summarizes changes in sedimentation rates at each contourite drift relative to changes at the boundaries, i.e., Arctic-N. Atlantic gradients in the atmospheric forcing, and heat and freshwater supply gradients between the North Atlantic and the North Pacific. The changes of the detrended sedimentation rates from the experiments have been scaled down to decadal values relative to representative changes at the boundaries. This makes the results for the different locations and different boundary conditions in each experiment comparable. It can be observed that the heat transport gradient between the North Atlantic and the North Pacific has the largest impact on sedimentation rates of most of the contourite drifts, followed by the precipitation gradient between the Arctic Ocean and the North Atlantic. In general, changes are more pronounced for increased gradients (DJF) than for decreased gradients (JJA) at the boundaries. This observation leads to the conclusion that sufficient gradients in the N. Pacific-Arctic-N. Atlantic oceanic-atmospheric system are necessary to maintain the general circulation dynamics in the ocean which is a documented concept for the region (Stigebrandt, 1984).

3.5 Considerations regarding the limits of the study

The final conclusions from our results (see Section 4) must be put into perspective of the model setup in order to evaluate the possibility for a quantitative application based on this study.

Most importantly, sediments in our experiments are of one uniform type only representing the dynamics of eroded and relocated material. Other sediment sources, such as pelagic and hemi-pelagic sediments, e.g. carbonate preservation, fluvial and glacial terrigeneous runoff, ice-rafted debris and aeolian input, are not included in the modeled processes. Especially the supply of Greenland bedrock material by glaciers can be of the same order as modern sedimentation rates in the Eirik Drift (Reyes et al., 2014).

However, sedimentation of these sources is predominately driven by atmospheric forcing. In order to reveal interdependencies between sedimentary processes and ocean dynamics it is rather advantageous that our model contains only one sediment source. Incorporating additional sediment sources will be necessary when the simulation of realistic paleo-states is aimed for.

It also has to be noted that the investigated area has been subject to major tectonic changes throughout the past millions of years which affected the depths and width of overflow sills and supply passages (e.g., Heirman et al., 2019; Uenzelmann-Neben and Gruetzner, 2018; Hu et al., 2015; Robinson et al., 2011; Hunter et al., 2007b). Most notably, the location of a mantle plume underneath the Greenland-Scotland-Ridge, causing oceanic crust to swell locally, is understood to have influenced deep water pathways in the past (Parnell-Turner et al., 2015). These variations of the bathymetry have not been included in this study which makes references to paleo-observations vague. Furthermore, bathymetric changes are known to alter tides drastically, as has been shown for the Arctic region in terms of the Arctic Megatides during the Last Glacial Maximum (Griffiths and Peltier, 2008). However, so far, in our model set up explicit tides are not included.

Therefore, further studies investigating sensitivity of North Atlantic contouritic sedimentation to topographic changes and consequential tidal variations may lead to a better understanding of the dominant factors for past variations of sedimentation intensity in the drift regions. Such information is crucial for the set up of a model for sedimentation in paleo-oceans.

4 Conclusions

We successfully simulated contouritic sedimentation in a new set up of a dynamically coupled ice-ocean-sediment model which produced statistically significant changes in sedimentation rates in response to changes at its atmospheric and lateral boundary conditions.

Furthermore, the results from Section 3 and Table 4 can be combined to form the following statements about the simulated deep water supply and contouritic sedimentation in the northern North Atlantic:

- Sedimentation in almost all contourite drifts is sensitive to climate conditions, being generally enhanced (reduced) under cold (warm) conditions.

- The sedimentation rate sensitivity appears to be stronger towards cold climate conditions than for warm conditions for most of the locations with an initial delay corresponding to the initial interannual sea ice growth during lasting cold conditions. This behavior supports the concept of sea ice extent to be the main driver of relocated deep water formation sites in the Nordic Seas.

- Deep water flows are modified by different climate conditions in terms of their pathways and intensity. This is especially the case for the Denmark Strait Overflow Water through the direct dependence on the formation of cold saline waters from the Arctic Ocean. The properties of these waters are substantially altered by changing sea ice volumes under different climate modes. The decrease of DSOW in JJA is in accordance with recent observations suggesting that warming Nordic Seas reduce overflows across the GISR, especially through the Denmark Strait.

- Sedimentation in the Eirik Drift does not appear to be solely sensitive to the supply of Denmark Strait Overflow Water. It may be equally influenced by the formation of Labrador Sea Water, especially during cold climate conditions, and ISOW. However, the various pathways of the latter are still not completely revealed.

- Labrador Sea Water is very likely to at least alter sedimentation rates in regions under its primary influence, as is apparently the case for Gloria Drift.

- Most notably, the intensity of gradients in atmospheric and different lateral boundaries appear to be the main driver of sedimentation rate sensitivity at North Atlantic contourite locations. The correlation is most pronounced for lateral heat supply and precipitation.

Acknowledgements

We are very grateful that this study received full funding by the Deutsche Forschungsgemeinschaft (DFG) as part of the priority program "Integrated Ocean drilling Program" (IODP) via contracts WE 6257/1-1, SA 2952/2-1 and Ue 49/19. We acknowledge the Norwegian Meteorological Institute sharing essential components of their former forecast model configuration "Arctic20km" for ROMS and thank Keguang Wang, Arne Melsom and Harald Engedahl for their helpful correspondence. During all numerical simulations and post-processing for this study we thankfully employed resources provided by Deutsches Klima Rechenzentrum (DKRZ).

References

Arakawa, A., and Lamb, V. R. (1977). Computational Design of the Basic Dynamical Processes of the UCLA General Circulation Model. *Methods in Computational Physics: Advances in Research and Applications*, *17*, 173–265. doi:10.1016/b978-0-12-460817-7.50009-4.

Avsic, T., Karstensen, J., Send, U., and Fischer, J. (2006). Interannual variability of newly formed Labrador Sea Water from 1994 to 2005. *Geophys. Res. Lett.*, *33*, 21–23. doi:10.1029/2006GL026913.

Berrisford, P., Dee, D., Fielding, K., Fuentes, M., Kallberg, P., Kobayashi, S., and Uppala, S. (2011). The ERA-Interim Archive Version 2.0. URL: https://www.ecmwf.int/node/8174.

Bianchi, G. G., and McCave, I. N. (2000). Hydrography and sedimentation under the deep western boundary current on Bjorn and Gardar Drifts, Iceland Basin. *Marine Geology*, *165*, 137–169. doi:10.1016/S0025-3227(99)00139-5.

Björk, G., Gustafsson, B. G., and Stigebrandt, A. (2001). Upper layer circulation of the Nordic Seas as inferred from the spatial distribution of heat and freshwater content and potential energy. *Polar Research*, *20*, 161–168. doi:10.3402/polar.v20i2.6513.

Blaas, M., Dong, C., Marchesiello, P., McWilliams, J. C., and Stolzenbach, K. D. (2007). Sediment-transport modeling on Southern Californian shelves: A ROMS case study. *Continental Shelf Research*, *27*, 832–853. doi:10.1016/j.csr.2006.12.003.

Blake-Mizen, K., Hatfield, R. G., Stoner, J. S., Carlson, A. E., Xuan, C., Walczak, M., Lawrence, K. T., Channell, J. E., and Bailey, I. (2019). Southern Greenland glaciation and Western Boundary Undercurrent evolution recorded on Eirik Drift during the late Pliocene intensification of Northern Hemisphere glaciation. *Quaternary Science Reviews*, *209*, 40–51. doi:10.1016/j.quascirev.2019.01.015.

Bower, A. S., Lozier, M. S., Gary, S. F., and Böning, C. W. (2009). Interior pathways of the North Atlantic meridional overturning circulation. *Nature*, *459*, 243–247. doi:10.1038/nature07979.

Broeker, W. (1991). The Great Ocean Conveyor. *Oceanography*, *4*, 79–89. doi:10.5670/oceanog.1991.07.

Budgell, W. P. (2005). Numerical simulation of ice-ocean variability in the Barents Sea region. *Ocean Dynamics*, *55*, 370–387. doi:10.1007/s10236-005-0008-3.

Channell, J. E. T., Kanamatsu, T., Sato, T., Stein, R., Zarikian, A., Malone, C. A., and the Expedition303/306 Scientists (2006). Expedition 303 Summary. *Proceedings of the Integrated Ocean Drilling Program*, *303/306*. doi:10.2204/iodp.proc.303306.101.2006.

Chapman, D. C. (1985). Numerical Treatment of Cross-Shelf Open Boundaries in a Barotropic Coastal Ocean Model. *Journal of Physical Oceanography*, *15*, 1060–1075. doi:10.1175/1520-0485(1985)015<1060:NTOCSO>2.0.CO;2.

Chough, S. K., and Hesse, R. (1984). Contourites from Eirik Ridge, south of Greenland. *Sedimentary Geology*, *41*, 185–199. doi:10.1016/0037-0738(84)90061-7.

Clark, P. U., Dyke, A. S., Shakun, J. D., Carlson, A. E., Clark, J., Wohlfarth, B., Mitrovica, J. X., Hostetler, S. W., and McCabe, A. M. (2009). The Last Glacial Maximum. *Science*, *325*, 710–714. doi:10.1126/science.1172873.

Dickson, B., Meincke, J., and Rhines, P. (2008). A General introduction. In B. Dickson, J. Meincke, and P. Rhines (Eds.), *Arctic-Subarctic Ocean Fluxes: Defining the Role of the Northern Seas in Climate* (pp. 1–13). Springer Netherlands. doi:10.1007/978-1-4020-6774-7_1.

Dobslaw, H., Bergmann-Wolf, I., Dill, R., Poropat, L., Thomas, M., Dahle, C., Esselborn, S., König, R., and Flechtner, F. (2017). A new high-resolution model of non-tidal atmosphere and ocean mass variability for de-aliasing of satellite gravity observations: AOD1B RL06. *Geophysical Journal International*, *211*, 263–269. doi:10.1093/GJI/GGX302.

Dowling, L. M., and McCave, I. N. (1993). Sedimentation on the Feni Drift and late Glacial bottom water production in the northern Rockall Trough. *Sedimentary Geology*, *82*, 79–87. doi:10.1016/0037-0738(93)90114-K.

Fairall, C. W., Bradley, E. F., Rogers, D. P., Edson, J. B., and Young, G. S. (1996). Bulk parameterization of air-sea fluxes for tropical oceanglobal atmosphere coupled-ocean atmosphere response experiment. *Journal of Geophysical Research: Oceans*, *101*, 3747–3764. doi:10.1029/95JC03205.

Faugères, J. C., Gonthier, E., Grousset, F., and Poutiers, J. (1981). The Feni Drift: The importance and meaning of slump deposits on the eastern slope of the Rockall Bank. *Marine Geology*, *40*, M49–M57. doi:10.1016/0025-3227(81)90138-9.

Faugères, J. C., Mézerais, M. L., and Stow, D. A. (1993). Contourite drift types and their distribution in the North and South Atlantic Ocean basins. *Sedimentary Geology*, *82*, 189–203. doi:10.1016/0037-0738(93)90121-K.

Faugères, J. C., Stow, D. A., Imbert, P., and Viana, A. (1999). Seismic features diagnostic of contourite drifts. *Marine Geology*, *162*, 1–38. doi:10.1016/S0025-3227(99)00068-7.

Fillon, R. H., and Duplessy, J. C. (1980). Labrador Sea bio-, tephro-, oxygen isotopic stratigraphy and Late Quaternary paleoceanographic trends. *Canadian Journal of Earth Sciences*, *17*, 831–854. doi:10.1139/e80-083.

Griffiths, S. D., and Peltier, W. R. (2008). Megatides in the Arctic Ocean under glacial conditions. *Geophys. Res. Lett.*, *35*, L08605. doi:10.1029/2008GL033263.

Gruber, N., Gloor, M., Mikaloff Fletcher, S. E., Doney, S. C., Dutkiewicz, S., Follows, M. J., Gerber, M., Jacobson, A. R., Joos, F., Lindsay, K., Menemenlis, D., Mouchet, A., Müller, S. A., Sarmiento, J. L., and Takahashi, T. (2009). Oceanic sources, sinks, and transport of atmospheric CO2. *Global Biogeochemical Cycles*, *23*, GB1005. doi:10.1029/2008GB003349.

Harris, C. K., and Wiberg, P. L. (1997). Approaches to quantifying long-term continental shelf sediment transport with an example from the northern California STRESS mid-shelf site. *Continental Shelf Research*, *17*, 1389–1418. doi:10.1016/S0278-4343(97)00017-4.

Haupt, B. J., Schäfer-Neth, C., and Stattegger, K. (1994). Modeling sediment drifts: A coupled oceanic circulation-sedimentation model of the northern North Atlantic. *Paleoceanography*, *9*, 897–916. doi:10.1029/94PA01437.

Heirman, K., Nielsen, T., and Kuijpers, A. (2019). Impact of Tectonic, Glacial and Contour Current Processes on the Late Cenozoic Sedimentary Development of the Southeast Greenland Margin. *Geosciences*, *9*, 157. doi:10.3390/geosciences9040157.

Holliday, N. P., Pollard, R. T., Read, J. F., and Leach, H. (2000). Water mass properties and fluxes in the Rockall Trough, 1975-1998. *Deep-Sea Research Part I: Oceanographic Research Papers*, *47*, 1303–1332. doi:10.1016/S0967-0637(99)00109-0.

Hu, A., Meehl, G. A., Han, W., Otto-Bliestner, B., Abe-Ouchi, A., and Rosenbloom, N. (2015). Effects of the Bering Strait closure on AMOC and global climate under different background climates. *Progress in Oceanography*, *132*, 174–196. doi:10.1016/j.pocean.2014.02.004.

Hunke, E. C., and Dukowicz, J. K. (1997). An Elastic-Viscous-Plastic Model for Sea Ice Dynamics. *Journal of Physical Oceanography*, *27*, 1849–1867. doi:10.1175/1520-0485(1997)027<1849:AEVPMF>2.0.CO;2.

Hunter, S. E., Wilkinson, D., Louarn, E., Nick McCave, I., Rohling, E., Stow, D. A., and Bacon, S. (2007a). Deep western boundary current dynamics and associated sedimentation on the Eirik Drift, Southern Greenland Margin. *Deep-Sea Research Part I: Oceanographic Research Papers*, *54*, 2036–2066. doi:10.1016/j.dsr.2007.09.007.

Hunter, S. E., Wilkinson, D., Stanford, J., Stow, D. A., Bacon, S., Akhmetzhanov, A. M., and Kenyon, N. H. (2007b). The Eirik Drift: A long-term barometer of North Atlantic deepwater flux south of Cape Farewell, Greenland. *Geological Society, London, Special Publication*, *276*, 245–263. doi:10.1144/GSL.SP.2007.276.01.12.

Johnson, G. C. (2008). Quantifying Antarctic Bottom Water and North Atlantic Deep Water volumes. *Journal of Geophysical Research: Oceans*, *113*. doi:10.1029/2007JC004477.

Jungclaus, J. H., Fischer, N., Haak, H., Lohmann, K., Marotzke, J., Matei, D., Mikolajewicz, U., Notz, D., and Von Storch, J. S. (2013). Characteristics of the ocean simulations in the Max Planck Institute Ocean Model (MPIOM) the ocean component of the MPI-Earth system model. *J. Adv. Model. Earth Syst.*, *5*, 422–446. doi:10.1002/jame.20023.

Köhl, A., Käse, R. H., Stammer, D., and Serra, N. (2007). Causes of changes in the Denmark strait overflow. *Journal of Physical Oceanography*, *37*, 1678–1696. doi:10.1175/JPO3080.1.

Kuhlbrodt, T., Griesel, A., Montoya, M., Levermann, A., Hofmann, M., and Rahmstorf, S. (2007). On the driving processes of the Atlantic meridional overturning circulation. *Rev. Geophys.*, *45*, RG2001. doi:10.1029/2004RG000166.

Lammers, R. B., Shiklomanov, A. I., Vörösmarty, C. J., Fekete, B. M., and Peterson, B. J. (2001). Assessment of contemporary Arctic river runoff based on observational discharge records. *Journal of Geophysical Research Atmospheres*, *106*, 3321–3334. doi:10.1029/2000JD900444.

Langehaug, H. R., Mjell, T. L., Otterå, O. H., Eldevik, T., Ninnemann, U. S., and Kleiven, H. F. (2016). On the reconstruction of ocean circulation and climate based on the Gardar Drift. *Paleoceanography*, *31*, 399–415. doi:10.1002/2015PA002920.

Lisiecki, L. E., and Raymo, M. E. (2005). A Pliocene-Pleistocene stack of 57 globally distributed benthic δ 18O records. *Paleoceanography*, *20*, 1–17. doi:10.1029/2004PA001071.

Liu, W. T., Katsaros, K. B., and Businger, J. A. (1979). Bulk parameterization of air-sea exchanges of heat and water vapor including the molecular constraints at the interface. *Journal of Atmospheric Sciences*, *36*, 1722–1735. doi:10.1175/1520-0469(1979)036<1722:BPOASE>2.0.CO;2.

MacLachlan, S. E., Elliott, G. M., and Parson, L. M. (2008). Investigations of the bottom current sculpted margin of Hatton Bank, NE Atlantic. *Marine Geology*, *253*, 170–184. doi:10.1016/j.margeo.2008.05.012.

Macrander, A., Käse, R. H., Send, U., Valdimarsson, H., and Steingrímur Jónsson (2007). Spatial and temporal structure of the Denmark Strait Overflow revealed by acoustic observations. *Ocean Dynamics*, *57*, 75–89. doi:10.1007/s10236-007-0101-x.

Macrander, A., Send, U., Valdimarsson, H., Jónsson, S., and Käse, R. H. (2005). Interannual changes in the overflow from the Nordic Seas into the Atlantic Ocean through Denmark Strait. *Geophys. Res. Lett.*, *32*, 1–4. doi:10.1029/2004GL021463.

Madsen, K. S., Rasmussen, T. A. S., Ribergaard, M. H., and Ringgaard, I. M. (2016). High resolution sea-ice modelling and validation of the Arctic with focus on South Greenland Waters, 2004-2013. doi:10.2312/polfor.2016.006.

Mason, E., Molemaker, J., Shchepetkin, A. F., Colas, F., McWilliams, J. C., and Sangrà, P. (2010). Procedures for offline grid nesting in regional ocean models. *Ocean Modelling*, . doi:10.1016/j.ocemod.2010.05.007.

Mastropole, D., Pickart, R. S., Valdimarsson, H., Våge, K., Jochumsen, K., and Girton, J. (2017). On the hydrography of Denmark Strait. *Journal of Geophysical Research: Oceans*, *122*, 306–321. doi:10.1002/2016JC012007.

McCartney, M. S. (1992). Recirculating components to the deep boundary current of the northern North Atlantic. *Progress in Oceanography*, *29*, 283–383. doi:10.1016/0079-6611(92)90006-L.

Meincke, J., Rudels, B., and Friedrich, H. J. (1997). The Arctic Ocean-Nordic Seas thermohaline system. *ICES Journal of Marine Science*, *54*, 283–299. doi:10.1006/jmsc.1997.0229.

Mellor, G. L., and Kantha, L. (1989). An Ice-Ocean Coupled Model. *Journal of Geophysical Research*, *94*, 937–954. doi:10.1029/jc094ic08p10937.

Mellor, G. L., and Yamada, T. (1982). Development of a turbulence closure model for geophysical fluid problems. *Rev. Geophys.*, *20*, 851–875. doi:10.1029/RG020i004p00851.

Müller-Michaelis, A., and Uenzelmann-Neben, G. (2014). Development of the Western Boundary Undercurrent at Eirik Drift related to changing climate since the early Miocene. *Deep Sea Research Part I: Oceanographic Research Papers*, *93*, 21–34. doi:10.1016/j.dsr.2014.07.010.

Müller-Michaelis, A., Uenzelmann-Neben, G., and Stein, R. (2013). A revised Early Miocene age for the instigation of the Eirik Drift, offshore southern Greenland: Evidence from high-resolution seismic reflection data. *Marine Geology*, *340*, 1–15. doi:10.1016/j.margeo.2013.04.012.

Orlanski, I. (1976). A simple boundary condition for unbounded hyperbolic flows. *Journal of Computational Physics*, *21*, 251–269. doi:10.1016/0021-9991(76)90023-1.

Papanicolaou, A. T. N., Elhakeem, M., Krallis, G., Prakash, S., and Edinger, J. (2008). Sediment Transport Modeling ReviewCurrent and Future Developments. *Journal of Hydraulic Engineering*, *134*, 1–14. doi:10.1061/(ASCE)0733-9429(2008)134:1(1).

Parnell-Turner, R., White, N., Mccave, I., Henstock, T., Murton, B., and Jones, S. (2015). Architecture of North Atlantic Contourite Drifts Modified by Transient Circulation of the Icelandic Mantle Plume. *Geochemistry, Geophysics, Geosystems*, *16*, 3414–3435. doi:10.1002/2015GC005947.

Rahmstorf, S. (1995). Bifurcations of the Atlantic thermohaline circulation in response to changes in the hydrological cycle. *Nature*, *378*, 145–149. doi:10.1038/378145a0.

Raymond, W. H., and Kuo, H. L. (1984). A radiation boundary condition for multidimensional flows. *Quarterly Journal of the Royal Meteorological Society*, *110*, 535–551. URL: http://doi.wiley.com/10.1002/qj.49711046414. doi:10.1002/qj.49711046414.

Rebesco, M., Hernández-Molina, F. J., Van Rooij, D., and Wåhlin, A. (2014). Contourites and associated sediments controlled by deep-water circulation processes: State-of-the-art and future considerations. *Marine Geology*, *352*, 111–154. doi:10.1016/j.margeo.2014.03.011.

Rebesco, M., Wåhlin, A., Laberg, J. S., Schauer, U., Beszczynska-Möller, A., Lucchi, R. G., Noormets, R., Accettella, D., Zarayskaya, Y., and Diviacco, P. (2013). Quaternary contourite drifts of the Western Spitsbergen margin. *Deep-Sea Research Part I: Oceanographic Research Papers*, *79*, 156–168. doi:10.1016/j.dsr.2013.05.013.

Reyes, A. V., Carlson, A. E., Beard, B. L., Hatfield, R. G., Stoner, J. S., Winsor, K., Welke, B., and Ullman, D. J. (2014). South Greenland ice-sheet collapse during Marine Isotope Stageâ 11. *Nature*, *510*, 525–528. doi:10.1038/nature13456.

Robinson, M. M., Valdes, P. J., Haywood, A. M., Dowsett, H. J., Hill, D. J., and Jones, S. M. (2011). Bathymetric controls on Pliocene North Atlantic and Arctic sea surface temperature and deepwater production. *Palaeogeography, Palaeoclimatology, Palaeoecology*, *309*, 92–97. doi:10.1016/j.palaeo.2011.01.004.

Røed, L., and Debernard, J. (2004). Description of an integrated flux and sea-ice model suitable for coupling to an ocean and atmosphere model. URL: http://met.no/filestore/MI-IM-Documentation.pdf.

Rothwell, R. G., and Rack, F. R. (2006). New techniques in sediment core analysis: An introduction. *Geological Society, London, Special Publication*, *267*, 1–29. doi:10.1144/GSL.SP.2006.267.01.01.

Rudels, B., Fahrbach, E., Meincke, J., Budéus, G., and Eriksson, P. (2002). The East Greenland Current and its contribution to the Denmark Strait overflow. *ICES Journal of Marine Science*, *59*, 1133–1154. doi:10.1006/jmsc.2002.1284.

Schweiger, A., Lindsay, R., Zhang, J., Steele, M., Stern, H., and Kwok, R. (2011). Uncertainty in modeled Arctic sea ice volume. *Journal of Geophysical Research: Oceans*, *116*. doi:10.1029/2011JC007084.

Shchepetkin, A. F., and McWilliams, J. C. (2005). The regional oceanic modeling system (ROMS): A split-explicit, free-surface, topography-following-coordinate oceanic model. *Ocean Modelling*, *9*, 347–404. doi:10.1016/j.ocemod.2004.08.002.

Sivkov, V. V., Dorokhova, E. V., and Bashirova, L. D. (2015). Contour currents of the North Atlantic during the last glacial cycle. *Oceanology*, *55*, 899–905. doi:10.1134/S0001437015060181.

Srivastava, S. P., Arthur, M. A., Clement, B., Aksu, A., Baldauf, J., Bohrmann, G., Busch, W., Cederberg, T., Cremer, M., Dadey, K., De Vernal, A., Firth, J., Hall, F., Head, M., Hiscott, R., Jarrard, R., Kaminski, M., Lazarus, D., Monjanel, A.-L., Nielsen, O. B., Stein, R., Thiebault, F., Zachos, J., Zimmerman, H., and Shipboard Scientific Party (1989). Proceedings of the Ocean Drilling Program Leg 105, Scientific Results. doi:10.2973/odp.proc.sr.105.1989.

Stanford, J. D., Rohling, E. J., Bacon, S., and Holliday, N. P. (2011). A review of the deep and surface currents around Eirik Drift, south of Greenland: Comparison of the past with the present. *Global and Planetary Change*, *79*, 244–254. doi:10.1016/j.gloplacha.2011.02.001.

Stigebrandt, A. (1984). The North Pacific: A Global-Scale Estuary. *Journal of Physical Oceanography*, *14*, 464–470. doi:10.1175/1520-0485(1984)014<0464:tnpags>2.0.co;2.

Stigebrandt, A. (1985). On the hydrographic and ice conditions in the northern North Atlantic during different phases of a glaciation cycle. *Palaeogeography, Palaeoclimatology, Palaeoecology*, *50*, 303–321. doi:10.1016/0031-0182(85)90074-4.

Stocker, T. F., Wright, D. G., and Broecker, W. S. (1992). The influence of high-latitude surface forcing on the global thermohaline circulation. *Paleoceanography*, *7*, 529–541. doi:10.1029/92PA01695.

Stoker, M. S. (2002). Late Neogene development of the UK Atlantic margin. *Geological Society, London, Special Publication*, *196*, 313–329. doi:10.1144/GSL.SP.2002.196.01.17.

The US Board on Geographic Names (2015). *The U.S. Board on Geographic names (USBGN) Advisory Committee on Undersea Features (ACUF). Report to GEBCO/SCUFN 28; 12-16 Oct, 2015*. Technical Report.

Uenzelmann-Neben, G., and Gruetzner, J. (2018). Chronology of Greenland Scotland Ridge overflow: What do we really know? *Marine Geology*, *406*, 109–118. doi:10.1016/j.margeo.2018.09.008.

Wåhlin, A. K. (2004). Topographic advection of dense bottom water. *Journal of Fluid Mechanics*, *510*, 95–104. doi:10.1017/S0022112004009590.

Wang, K., Debernard, J., Sperrevik, A. K., Isachsen, P. E., and Lavergne, T. (2013). A combined optimal interpolation and nudging scheme to assimilate OSISAF sea-ice concentration into ROMS. *Annals of Glaciology*, *54*, 8–12. doi:10.3189/2013AoG62A138.

Warner, J. C., Sherwood, C. R., Signell, R. P., Harris, C. K., and Arango, H. G. (2008). Development of a three-dimensional, regional, coupled wave, current, and sediment-transport model. *Computers & Geosciences*, *34*, 1284–1306. doi:10.1016/j.cageo.2008.02.012.

Zou, S., Bower, A., Furey, H., Susan Lozier, M., and Xu, X. (2020). Redrawing the Iceland-Scotland Overflow Water pathways in the North Atlantic. *Nature Communications*, *11*, 1890. doi:10.1038/s41467-020-15513-4.